Last ice sheet recession and landscape emergence above sea level in east-central Sweden, evaluated using *in situ cosmogenic* ^{14}C from quartz

Bradley W. Goodfellow[1*]
Arjen P. Stroeven[2,3]
Nathaniel A. Lifton[4,5]
Jakob Heyman[6]
Alexander Lewerentz[1]
Kristina Hippe[7]
Jens-Ove Näslund[8]
Marc W. Caffee[4,5]

[1]Geological Survey of Sweden
[2]Department of Physical Geography, Stockholm University
[3]Bolin Centre for Climate Research, Stockholm University
[4]Department of Earth, Atmospheric, and Planetary Sciences, Purdue University
[5]Department of Physics and Astronomy, Purdue University
[6]Department of Earth Sciences, University of Gothenburg
[7]Umweltplanung Dr. Klimsa
[8]Swedish Nuclear Fuel and Waste Management Company (SKB)

*Corresponding author: bradley.goodfellow@sgu.se

Abstract

In situ cosmogenic ^{14}C (*in situ* ^{14}C) in quartz provides a recently developed tool to date exposure of bedrock surfaces up to ~25,000 years. From outcrops located in east-central Sweden, we test the accuracy of *in situ* ^{14}C dating against (i) a relative sea level (RSL) curve constructed from radiocarbon dating of organic material in isolation basins, and (ii) the timing of local deglaciation constructed from a clay varve chronology complemented with traditional radiocarbon dating. Five samples of granitoid bedrock were taken along an elevation transect extending southwestwards from the Baltic Sea coast near Forsmark. Because these samples derive from bedrock outcrops positioned below the highest postglacial shoreline, they target the timing of progressive landscape emergence above sea level. In contrast, *in situ* ^{14}C concentrations in an additional five samples taken from granitoid outcrops above the highest postglacial shoreline, located 100 km west of Forsmark, should reflect local deglaciation

ages. The ten *in situ* ^{14}C measurements provide robust age constraints that, within uncertainties, compare favorably with the RSL curve and with the local deglaciation chronology. These data demonstrate the utility of *in situ* ^{14}C to accurately date ice sheet deglaciation, and durations of postglacial exposure, in regions where cosmogenic ^{10}Be and ^{26}Al routinely return complex exposure results.

1. Introduction

The pacing of retreat of ice sheets in North America and Eurasia since their maximum expansion during the last glaciation remains an active research field (e.g., Hughes et al., 2016; Stroeven et al., 2016; Patton et al., 2017; Dalton et al., 2020, 2023). Understanding the triggers and processes causing the demise of these ephemeral ice sheets yields the best blueprint for understanding the future behavior of the Greenland and Antarctic ice sheets in a warming climate. Coupling the behavior of deglaciating ice sheets over the course of the Late Glacial and early Holocene to increasingly precise climate reconstructions, including ~~and~~ climatic events, requires increased precision in ice sheet reconstructions (e.g., Bradwell et al., 2021). ~~Increased~~ Pprecision can be ~~achieved~~ enhanced through ~~a~~ coupling ~~of~~ geomorphological mapping of ice sheet margins (such as moraines, grounding zone wedges, lateral meltwater channels, and ice-dammed lake shorelines and spillways) with numerical field constraints from a diverse array of dating techniques (e.g., Stroeven et al., 2016; Bradwell et al., 2021; Regnéll et al., 2023).

Ice sheet reconstructions, especially in North America, have ~~attained a high level of detail~~become highly detailed through radiocarbon dating (Dyke et al., 2002; Dalton et al., 2020). With the advance of offshore imaging of glacial geomorphology (Greenwood et al., 2017, 2021; Bradwell et al., 2021), radiocarbon dating has received a renewed upswing in recent years (e.g., Dalton et al., 2020; Bradwell et al., 2021). However, large ~~tracts of~~ landscape areas lack radiocarbon age constraints on ice sheet retreat ~~simply due to~~ because of an absence ~~lack~~ of datable organic material. Fortunately, optically - stimulated luminescence ages on buried sand layers (e.g., Alexanderson et al., 2022) and cosmogenic nuclide apparent exposure ages on exposed bedrock and erratics have narrowed some of the gaps (e.g., Hughes et al., 2016; Stroeven et al., 2016; Dalton et al., 2023). In studies using cosmogenic nuclides, an 'apparent' exposure age is derived from a simple calculation from the nuclide concentration under consideration (Lal, 1991; Gosse and Phillips, 2001). ~~However,~~ Ccorrectly interpreting the exposure age relies on modelling that considers geological factors that can reduce the nuclide concentration relative to the time since initial subaerial exposure (such as erosion and burial by glacial ice, water, snow, and/or soil; Gosse and Phillips, 2001; Schildgen et al., 2005; Ivy-Ochs and Kober, 2008). Exposure dating is the only technique available in regions where ice sheet erosion has left the surface bare or covered by a thin drape of till. Kleman et al. (2008) show that for Fennoscandia,

these conditions are widespread in coastal regions where ice accelerated towards its streaming sectors and where wave wash during glacial rebound further thinned or removed pre-existing sediment covers.

Coastal sectors in formerly glaciated regions provide sites important to the study of paleoglaciology. They offer an abundance of bedrock exposures from which patterns and processes of subglacial erosion can be studied through cosmogenic nuclide exposure dating (e.g., Hall et al., 2020). Also, because of the interplay with postglacial sea level, coastal areas yield data on glacioisostatic rebound that are critical to geodynamic modelling of Earth rheology and thicknesses of former ice sheets (e.g., Lambeck et al. (1998, 2010) and Patton et al. (2017), for Fennoscandian examples). Geodynamic models require validation against measurements of vertical crustal motion (Steffen and Wu, 2011), such as those provided by recent global positioning system (GPS) measurements (e.g., Lidberg et al., 2010) and postglacial records of crustal rebound afforded by relative sea level (RSL) curves (e.g., Påsse and Andersson, 2005). The construction of RSL curves, detailing the history of land surface emergence from sea level, is traditionally done using either sediments accumulated in isolation basins at different elevations above sea level or by dating uplifted gravel beach ridges. Typically, isolation basins, and their sediments, show a progression from marine, to brackish, and finally to freshwater environments as ~~their bedrock sills~~ they are uplifted through tidal levels (Long et al., 2011). Histories of land uplift above sea level are documented using micro- and macrofossil analyses of isolation basin sediments and radiocarbon dating on macrofossils (Romundset et al., 2011). Uplifted beach ridges can be radiocarbon dated from a variety of materials (Blake, 1993) but most confidently from driftwood, whalebone, and shells (e.g., Dyke et al., 1992). Gravel beach ridges have also been investigated using OSL and ^{10}Be exposure dating even though, other than the highest beach ridge, they may be prone to clast reworking (Briner et al., 2006; Simkins et al., 2013; Bierman et al., 2018). A distinct advantage of constructing RSL curves using cosmogenic nuclides is that land surface emergence above sea level may be additionally dated from boulders (Briner et al., 2006) or bedrock (Bierman et al., 2018).

The potential for cosmogenic surface exposure dating of last ice sheet retreat in recently glaciated low-relief cratonic landscapes would seemingly be high because of the frequent outcropping of glacially sculpt~~ur~~ed quartz-bearing crystalline bedrock. However, the ice sheet may have been either non-erosive or erosion was insufficiently deep to remove all the cosmogenic nuclide inventory from previous exposure periods. Apparent ages are therefore often older than indicated by radiocarbon dating (Heyman et al., 2011; Stroeven et al., 2016) because they include a component of nuclide inheritance. Apparent ages younger than indicated by radiocarbon dating can also occur if sampled rock surfaces have been shielded, for example by sediments, following deglaciation. Concentrations of ^{10}Be and ^{26}Al, in either bedrock or erratic boulders, ~~therefore~~ often reflect complex exposure histories rather than simple deglacial exposure durations (Heyman et al., 2011; Stroeven et al., 2016).

In this study we use ^{14}C produced *in situ* in quartz-bearing bedrock (*in situ* ^{14}C) because it potentially circumvents an overt reliance on the need for deep erosion (>3 m) to remove the inherited signal from previous exposure periods (Gosse and Phillips, 2001). The reason for this is that, Because of its short half-life of 5700 ± 30 years, nuclide inherited *in situ* ^{14}Cance will have largely decayed away if ice sheet burial at investigated sites during the last glacial phase (marine isotope stage 2; MIS2) exceeded 25-30 ka, that is, ca. 5 half-lives (Briner et al., 2014).

Some studies assessing changes in glacier and ice sheet extents over Late Glacial to Holocene timescales have used *in situ* ^{14}C (Miller et al., 2006; Fogwill et al., 2014; Hippe et al., 2014; Schweinsberg et al., 2018; Pendleton et al., 2019; Young et al., 2021; Schimmelpfennig et al., 2022). In such these studies, *in situ* ^{14}C has been applied with other nuclides with longer half-lives, in particular ^{10}Be, to unravel complex histories of glacier advance and retreat (e.g., Goehring et al., 2011) and spatial patterns in glacial erosion in mountainous terrain (e.g., Steinemann et al., 2021). However, Eextensive regions formerly covered by ice sheets are characterized by low relief, and low elevation terrain., Tand the effectiveness of *in situ* ^{14}C in dating ice sheet retreat in these non-alpine settings and in quantifying shoreline displacement from bedrock samples has not been previously assessed. The aim of this study is therefore to validate the use of ^{14}C formed *in situ* in bedrock as a reliable chronometer by evaluating its performance in duplicating (i) a previously-established Holocene RSL curve based on radiocarbon dating (Hedenström and Risberg, 2003; SKB, 2020) and (ii) the timing of deglaciation above the highest (post-glacial) shoreline in nearby east-central Sweden according to reconstructions of deglaciation of the last ice sheet (Hughes et al., 2016; Stroeven et al., 2016).

2. Study Area

Our study is focused on a region that includes low elevation, low relief, Forsmark-Uppland and adjoining higher elevation and relief Dalarna-Gävleborg in east-central Sweden (Fig. 1). This region was selected because Forsmark is the location of a planned geological repository for spent nuclear fuel (e.g., SKB 2022). As such, this region has been intensively studied and has a wealth of and therefore also has abundant geologic data relevant to our study. This includes in-depth analyses of bedrock and environmental properties, including influences of glacial and postglacial processes (e.g., Lönnqvist and Hökmark, 2013; Hall et al., 2019; Moon et al., 2020; SKB, 2020).

From spatio-temporal ice sheet reconstructions by Kleman et al. (2008), the study area was glaciated 16-20 times for a total duration of c. 330 kyr over the past 1 Ma. The last deglaciation of the study area is well-constrained by two recent reconstructions that differ in their approach (Hughes et al., 2016; Stroeven et al., 2016). The Hughes et al. (2016) reconstruction is explicitly basedrelies primarily upon on chronological constraints supplied ,from radiocarbon, thermal luminescence, optically stimulated

luminescence (OSL), infrared stimulated luminescence, electron spin resonance, terrestrial cosmogenic nuclide (TCN), and U-series dating. Published landform data, mostly with respect to end moraines and generally accepted correlations of ice-margin positions between individual moraines, provide complementary evidence. ~~but~~ In contrast, the Stroeven et al. (2016) reconstruction combines geomorphological constraints for ice sheet margin outlines, including ice-marginal depositional landforms and meltwater channels, ice-dammed lakes, eskers, lineations, and striae, -with chronological constraints supplied by radiocarbon, varve, OSL, and TCN dating. Whereas Hughes et al. (2016) reconstruct ice sheet retreat every 1 ka, and for every ice margin plot its position as "most credible", "min", and "max", Stroeven et al. (2016) present ice margin positions for every 100 years inside the Younger Dryas standstill position (Stroeven et al., 2015). These marginal positions are temporally and spatially defined by the "Swedish Time Scale" clay varve record along the Swedish east coast (De Geer, 1935, 1940; Strömberg, 1989, 1994; Brunnberg, 1995; Wohlfarth et al., 1995). From Stroeven et al. (2016), the last deglaciation of the study area occurred 10.8 ± 0.3 ka BP, which overlaps the timing of deglaciation of the study area from Hughes et al. (2016), within uncertainty (Fig. 1). The highest postglacial shoreline in east-central Sweden is located at a present elevation of ~200 m a.s.l. in Dalarna-Gävleborg, ~100 km west of Forsmark (SGU, 2015). The exposure duration of bedrock above the highest postglacial shoreline ~~therefore~~ represents the time since local deglaciation. Hence, *in situ* ^{14}C ages from bedrock above the highest postglacial shoreline should conform to the reconstructed deglaciation age of 10.8 ± 0.3 ka from Stroeven et al. (2016).

Below the highest postglacial shoreline, in the Forsmark-Uppland region, the last deglaciation occurred in a marine environment and the landscape has progressively emerged above sea level through postglacial isostatic uplift. A RSL curve constructed from radiocarbon dating of basal organic sediments trapped in isolation basins along elevation transects describes the progressive emergence of the Forsmark-Uppland landscape above sea level (Robertsson and Persson, 1989; Risberg, 1999; Bergström, 2001; Hedenström and Risberg, 2003; Berglund, 2005; SKB, 2020). Ages calculated from *in situ* ^{14}C from bedrock outcrops along an elevation transect would then mirror the Forsmark RSL curve for their corresponding elevations (but be slightly older because of nuclide production through shallow water before emergence).

A potential complication to the accurate exposure age dating of bedrock surfaces using *in situ* ^{14}C in east-central Sweden is that the most recent period of ice sheet burial may not have been sufficiently long to decay ~~the~~ any *in situ* ^{14}C inventory inherited from ~~preceding~~ prior exposure. Here, the extent of the Fennoscandian Ice Sheet during interstadial MIS3 and the timing of ice advance across the Forsmark region during late MIS3 are crucially important. Kleman et al. (2020) have identified ice-free conditions around Idre (330 km NW, up-ice, of our study area; Fig. 1) between 55 ka and 35 ka, which implies inundation of our study area by ice after 35 ka. Combined with a well-constrained final

deglaciation age of 10.8±0.3 ka (Stroeven et al. 2016), it appears that our study area has most recently (during MIS2) been inundated by glacial ice for at most 24 ka. This inference is in line with results from ice sheet modelling indicating a 22 kyr duration of ice-cover at Forsmark during MIS2 (SKB, 2020). Consequently, it is possible that *in situ* ^{14}C concentrations may reflect subaerial exposure of bedrock in our study area during MIS3 in addition to Holocene exposure, resulting in an offset towards older ages relative to the RSL curve for Forsmark (Hedenström and Risberg, 2003; SKB, 2020) and the deglaciation chronologies of Hughes et al. (2016) and Stroeven et al. (2016).

3. Methods

3.1. Sampling of bedrock outcrops for *in situ* ^{14}C measurement

We used the following sampling strategy to evaluate the accuracy of bedrock exposure ages derived from *in situ* ^{14}C against the Forsmark RSL curve and the deglaciation of the last ice sheet in east-central Sweden. A rigorous scheme was applied to ensure that we avoided sampling quartz altered through hydrothermal processes that is likely to occur in major pegmatite intrusions, outcrops located in major deformation zones, and outcrop-scale veins, fractures, and adjacent rock volumes. Consequently, sampling was done on outcrops of metagranitoid from the early-Svecokarelian GDG-GSDG suite that dominates the Bergslagen lithotectonic unit (Stephens and Jansson, 2020). A petrological examination using transmitted light polarization microscopy was applied to thin sections to ascertain that the quartz was unlikely to contain multi-fluid phase, vapour phase, or solid-phase inclusions. All samples were collected using an angle grinder, which permits sampling of hard crystalline bedrock isolated from outcrop edges, fractures, and quartz veins, and consistently limits sample thicknesses to 3 cm.

We collected a total of ten samples for *in situ* ^{14}C analyses. Five of these were collected along a SW-NE transect near Forsmark (Fig. 1b). These outcrops were chosen because they span an elevation gradient of 9.4–56.0 m a.s.l. and exposure ages derived from *in situ* ^{14}C can therefore be evaluated against the Forsmark RSL curve. We collected a further five samples from locations above the highest shoreline (Fig. 1a) to determine the age of local deglaciation for comparison with published deglaciation chronologies (Hughes et al., 2016; Stroeven et al., 2016). Sample locations were logged on a 2 m-resolution LiDAR digital elevation model (DEM) displayed in ArcGIS 10 on a tablet computer. A GPS add-in tool in ArcGIS 10 was used to record positional data, within a horizontal precision of 2 m. The elevation of each sample location was extracted from the DEM and has a precision of tens of centimetres. The influence of these minor positional uncertainties on our ^{14}C calculations is trivial and none of the sample sites is influenced by topographic shielding that could reduce the accumulation of ^{14}C in bedrock.

Each sampled bedrock outcrop formed a local topographic high, which minimizes the risk of burial by soil and snow (Supplement 1). Moss mats were present on all sampled outcrops. Although we avoided sampling bedrock that was moss-covered, we cannot be certain that moss mats did not formerly cover the sample sites. Given a compressed thickness of 0.5 cm and an estimated density of 0.7 g $/$cm^{-3}, this may have contributed to a shielding of the sampled rock surfaces of 0.35 g $/$cm^{-2}, which is negligible and is therefore excluded from our age inferences.

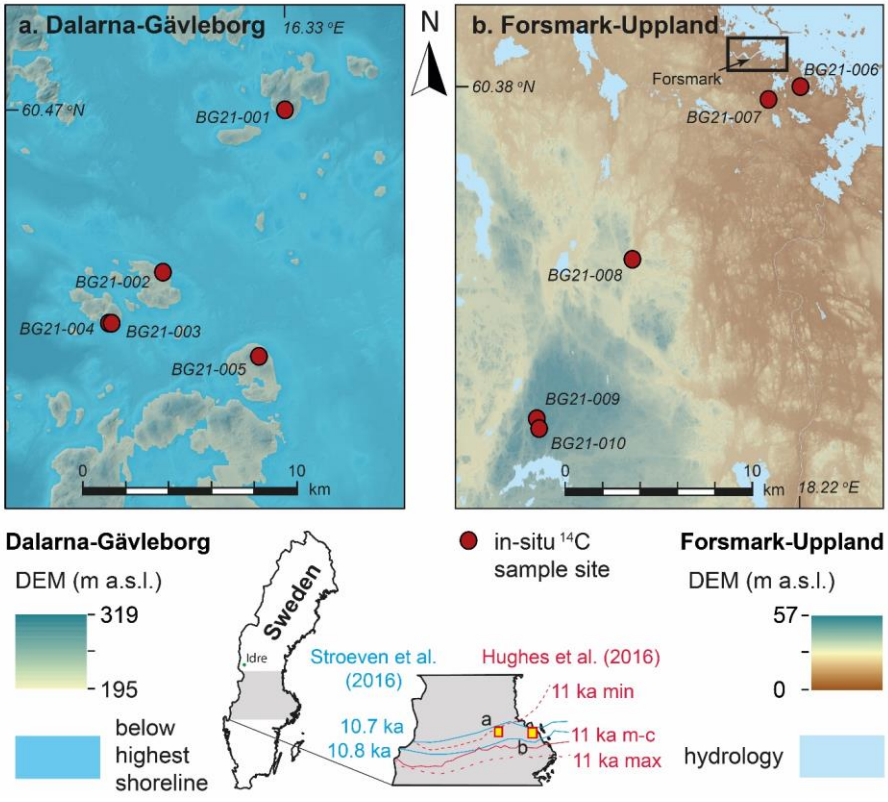

Figure 1. Sample locations for *in situ* ^{14}C dating in **(a)** Dalarna-Gävleborg and **(b)** Forsmark-Uppland. The five Dalarna-Gävleborg sample sites are located on what were islands above the highest postglacial shoreline (shown), whereas the five sample sites from Forsmark-Uppland are located below the highest shoreline (not shown because the entire area was submerged). See inset maps for locations of panels a and b and for the 10.7 ka BP and 10.8 ka BP retreat isochrones (blue) from Stroeven et al. (2016) and 11 ka BP (most-credible, minimum, and maximum) retreat isochrones (red) from Hughes et al. (2016). The rectangle in panel b approximately indicates the site selected for the planned geological repository for spent nuclear fuel at Forsmark. DEM with 2 m resolution, from LiDAR data, Lantmäteriet.

3.2. Laboratory preparation for accelerator mass spectrometry (AMS)

Samples were physically and chemically processed at the Purdue Rare Isotope Measurement Laboratory (PRIME Lab) at Purdue University, U.S.A. Concentrations of *in situ* ^{14}C were determined from purified quartz separates through automated procedures (Lifton et al., 2023). Approximately 5 g of quartz from each sample was added to a degassed $LiBO_2$ flux in a re-usable 90% Pt/10% Rh sample boat and heated to 500 °C for one hour in ca. 6.7 kPa of Research Purity O_2 to remove atmospheric contaminants, which were discarded. The sample was then heated to 1100 °C for three hours to dissolve the quartz and release the *in situ* ^{14}C, again in an atmosphere of ca. 6.7 kPa of Research Purity O_2 to oxidize any evolved carbon species to CO_2. The CO_2 from the 1100 °C step was then purified, measured quantitatively, and converted to graphite for ^{14}C AMS measurement at PRIME Lab (Lifton et al., 2023). To test for data reproducibility, sample BG21-002 was randomly selected to undergo laboratory preparation and AMS a second time. Measured concentrations of *in situ* ^{14}C are calculated from the measured isotope ratios via AMS following Hippe and Lifton (2014) (Table 1).

3.3. Exposure age calculations

The expage calculator version 202403~~312~~ (http://expage.github.io/calculator) is used to calculate apparent exposure ages. It is based on the original CRONUS calculator v. 2 (Balco et al., 2008), the LSDn production rate scaling (Lifton et al., 2014), and the CRONUScalc calculator (Marrero et al., 2016), using the geomagnetic framework of Lifton (2016) with the SHA.DIF.14k model for the last 14 kyr. Exposure ages are calculated using resulting time-varying ^{14}C production rates accounting for decay and interpolated to match the measured ^{14}C concentration. The production rate from muons is calibrated against the Leymon High core ^{14}C data of Lupker et al. (2015) and the production rate from spallation is calibrated against updated global ^{14}C production rate calibration data (Schimmelpfennig et al., 2012; Young et al., 2014; Lifton et al., 2015; Borchers et al., 2016; Phillips et al., 2016; Koester and Lifton, 2023, corrigendum in prep). This calibration is done iteratively for spallation and muons to reach convergence, using the expage production rate calibration methods (Fig. 2).

Exposure age calculations along the Forsmark-Uppland transect account for ^{14}C production during emergence through shallow water. ~~However, B~~burial of sampled surfaces by snow is excluded from the age calculations for all sample sites because we neither know how snow burial depths and durations vary between sites nor vary through time. The effect of snow burial would be to slightly decrease cosmogenic nuclide production in the underlying rock surface (Schildgen et al., 2005) and we have minimized this effect through our sampling strategy.

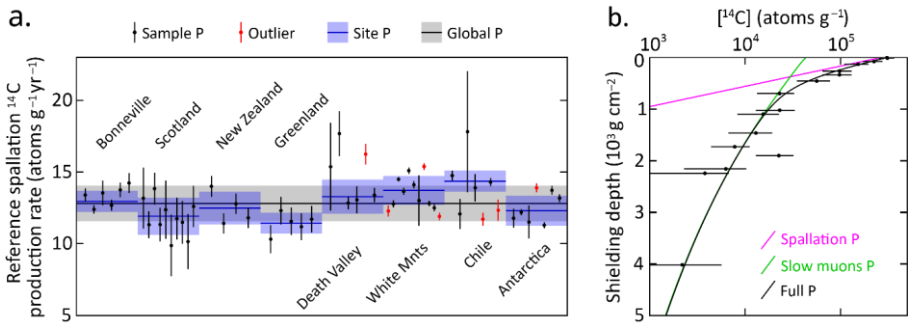

Figure 2. Production rate calibration of ^{14}C in quartz. **(a)** Reference spallation ^{14}C production rate calibration based on data from Schimmelpfennig et al. (2012), Young et al. (2014), Lifton et al. (2015), Borchers et al. (2016), and Phillips et al. (2016), corrected per Hippe and Lifton (2014) and compiled in Koester and Lifton (2023). An uncertainty-weighted production rate is calculated for each of the eight sites. Outliers, which are not included in the uncertainty-weighted production rates, are determined based on the requirement that there should be at least three samples yielding a reduced chi-square statistic (X_R^2) with a p-value of at least 0.05 for the assumption that the individual production rates from a site are derived from one normal distribution. For X_R^2, but not the uncertainty-weighting, we use the largest of the sample-specific production rate uncertainty based on the ^{14}C concentration uncertainties and 5% of the sample production rate. This procedure does not punish samples with low measurement uncertainties, which otherwise risk exclusion as outliers. We adopt a global reference spallation ^{14}C production rate of ~~13.35~~12.81 ±~~1.13~~1.25 atoms g^{-1} yr^{-1}, calculated as the arithmetic mean of the eight site production rates with the uncertainty being based on an uncertainty-weighted deviation of all included single sample production rates, excluding outliers. **(b)** Calibration of ^{14}C production rate from muons based on the data of Lupker et al. (2015). The calibration is based on the method used in the CRONUScalc calculator (Marrero et al., 2016; Phillips et al., 2016). The figure shows the best fit ^{14}C concentration profiles produced from spallation, slow muons, and full production. The best fit yields near zero production from fast muons (cf. Lupker et al., 2015). The production rate calibration has been carried out using the expage-202403~~306~~ calculator in an iterative way to make the global reference spallation ^{14}C production rate converge with the production rate from muons.

4. Results

Analytical results for *in situ* ^{14}C samples and procedural blanks are presented in Table 1. The mean and standard deviation are used to correct measured ^{14}C sample inventories (Table 1) because procedural blanks are well-constrained during the analytical time frame. Inferred ages for the five *in situ* ^{14}C samples from the Forsmark-Uppland transect (i.e., below the highest postglacial shoreline) are shown relative to

277 the Holocene RSL curve for Forsmark and the expected *in situ* ^{14}C exposure age curve considering
278 subaqueous cosmogenic nuclide production (Figure 3; Table~~s 1 and~~ 2). Exposure age uncertainties are
279 large with internal uncertainties (measurement uncertainties; Balco et al., 2008) of 5-9% and external
280 uncertainties of ~~12-20~~13-25% (also including production rate uncertainties, which are high relative to
281 ^{10}Be (Borchers et al., 2016; Phillips et al., 2016). Apparent exposure ages increase consistently with
282 elevation and match expected ages within uncertainty. The two highest samples have near-identical
283 apparent exposure ages and elevations. However, these samples provide independent ages because
284 they are horizontally separated by 624 m (Figure 1b). There is good agreement between ages inferred
285 from these *in situ* ^{14}C data and the RSL curve constructed from organic radiocarbon dating of isolation
286 events (Hedenström and Risberg, 2003; SKB, 2020).

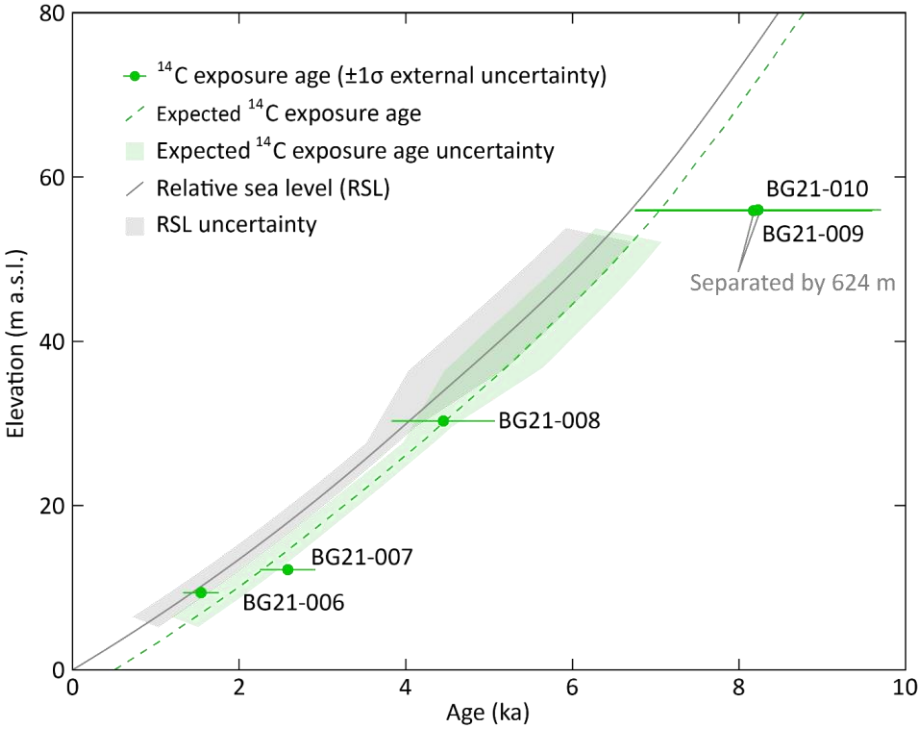

287

288 **Figure 3**. Apparent ^{14}C exposure ages for five Forsmark samples from below the highest shoreline (Fig.
289 1b; Table 2) with 1σ external uncertainties. The expected exposure ages are calculated assuming the RSL
290 curve is correct, the ^{14}C spallation production rate is correct, partial exposure as the sample approaches
291 the water surface, and full post-glacial exposure for the duration above sea level. Hence, the expected
292 exposure age curve is a few hundred years older than the RSL curve. The RSL curve is from SKB (2020)
293 and uncertainties for the 1–6 ka interval are calculated from the original radiocarbon data in Hedenström

and Risberg (2003). The RSL uncertainty envelope is also transposed onto the expected exposure age curve.

Apparent exposure ages for the five *in situ* ^{14}C samples located above the highest shoreline in Dalarna and Gävleborg (Fig. 1a) are shown in Figure 4 and Table 2. The weighted mean age from all five samples is 11.~~92~~ ± 1.~~53~~ ka. These data display a X_R^2 of 1.78 and a p-value of 0.13 based on 1σ internal uncertainties ~~(Fig. 4a)~~, which does not support a rejection of the hypothesis that the apparent exposure ages represent the same population. In addition to the samples being from the same population, the exposure ages are consistent, within uncertainty, with the expected deglaciation age of 10.8 ± 0.3 ka (Stroeven et al. 2016). Replicate measurements on sample BG21-002 closely agree and an age based on a weighted mean ^{14}C concentration is shown in Figure 4. ~~Sample BG21-001 provides the youngest apparent age but, because this sample was from a low-profile outcrop (Supplement 1), this age may reflect partial shielding of the sampled bedrock surface by a past shallow soil cover or perhaps a deeper snow cover than the other sites. We therefore consider this sample as least likely to provide a reliable age. Removing this sample from consideration indicates that the remaining four sample sites are more clustered, with an older weighted mean age of 11.612.4 ± 1.31 ka, which displays a X_R^2 of 0.423 and a p-value of 0.743 based on 1σ internal uncertainties (Fig. 4b).~~

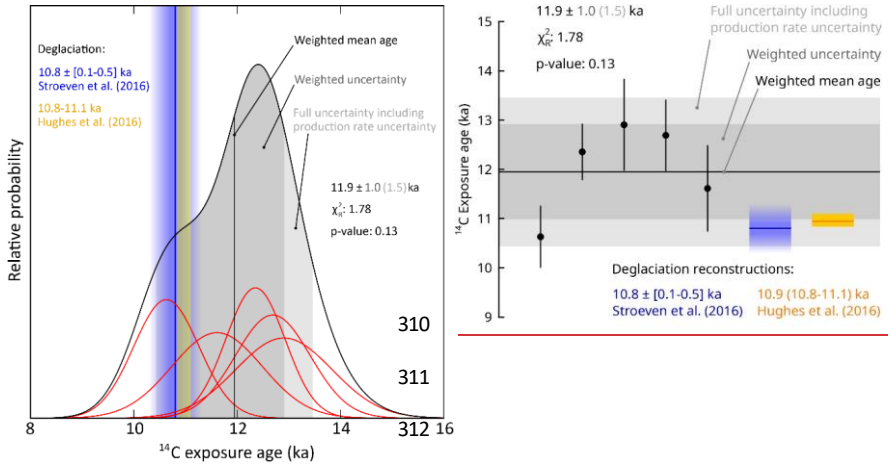

Figure 4. ~~Summed P~~probability ~~density plots~~distributions ~~of the E~~exposure ages from samples above the highest shoreline (Fig. 1a; Table 2). The individual samples (~~red curves~~filled black circles) display 1σ internal uncertainty (measurement uncertainty; black lines). For the repeat sample BG21-002, the exposure age is calculated with a weighted mean ^{14}C concentration using a 2% uncertainty. ~~**(a)** The probability density and data for all five samples. For the full set of samples, T~~the cosmogenic nuclide ages yield a reduced chi-square (X^2_R) of 1.78 and a p-value of 0.13 based on internal uncertainties, which indicates that they are from the same population. The color gradient for the Stroeven et al. (2016) deglaciation chronology indicates the 0.1–0.5 ka uncertainty range, whereas the uncertainty for the Hughes et al. (2016) chronology reflects the maximum and minimum estimates for deglaciation of the study area, which are unequally distributed around the most credible estimate (orange line). ~~**(b)** The probability density and data with sample BG21-001 excluded as an outlier. These cosmogenic nuclide ages yield a X^2_R of 0.423 and a p-value of 0.743 based on internal uncertainties, which again indicate that they are from the same population. All ages are referenced to the sampling year 2021. The weighted ages of 11.92 ± 1.53 ka and 11.612.4 ± 1.31 ka both overlap with the deglaciation age from Stroeven et al. (2016).~~

Formatted Table

Formatted: Justified

Formatted: Indent: First line: 0,3 cm

Formatted: Indent: First line: 0,25 cm

Table 1. Extraction and measuremen[illegible] *in situ* ^{14}C at PRIME

Sample ID	PCEGS #[a]	PLID[b]	M Qua[illegible] g)	C yield (μg)	Diluted mass C (μg)	Split ss C μg)	$\delta^{13}C^{c}$ (‰$_{VPDB}$)	$^{14}C/^{13}C$ (10^{-11})	$^{14}C/C_{total}$ (10^{-13})	^{14}C (10^{6} at)	$[^{14}C]$ (10^{5} at g^{-1})[d]
BG21-001	146	202101960	5[illegible]	5.0 ± 0.1	393.8 ± 4[illegible]	3 ± 4.6	-45.9 ± 0.2	0.3399 ± 0.0075	0.3412 ± 0.0079	0.6177 ± 0.0179	1.2296 ± 0.0357
BG21-002	147	202101961	5[illegible]	7.8 ± 0.1	303.3 ± 3[illegible]	4 ± 3.6	-44.8 ± 0.2	0.4555 ± 0.0096	0.4623 ± 0.0102	0.6470 ± 0.0181	1.2879 ± 0.0360
BG21-003	148	202101962	5[illegible]	17.6 ± 0.3	303.4 ± 3[illegible]	5 ± 3.6	-43.9 ± 0.2	0.4633 ± 0.0108	0.4709 ± 0.0113	0.6604 ± 0.0197	1.3180 ± 0.0393
BG21-002R	150	202201473	5[illegible]	7.7 ± 0.1	305.3 ± 3[illegible]	4 ± 3.6	-45.2 ± 0.2	0.4558 ± 0.0135	0.4624 ± 0.0142	0.6519 ± 0.0237	1.2931 ± 0.0470
BG21-004	152	202101963	5[illegible]	11.9 ± 0.2	305.7 ± 3[illegible]	8 ± 3.6	-44.6 ± 0.2	0.4618 ± 0.0079	0.4691 ± 0.0083	0.6630 ± 0.0159	1.3105 ± 0.0314
BG21-005	153	202101964	5[illegible]	4.6 ± 0.1	304.5 ± 3[illegible]	3 ± 3.6	-45.4 ± 0.2	0.4600 ± 0.0127	0.4667 ± 0.0134	0.6566 ± 0.0225	1.2935 ± 0.0444
BG21-006	155	202101965	5.06572	5.5 ± 0.1	306.8 ± 3.7	297.8 ± 3.6	-45.2 ± 0.2	0.1277 ± 0.0056	0.1172 ± 0.0059	0.1243 ± 0.0101	0.2453 ± 0.0199

Table 1. *In situ* ^{14}C sample measurement details

Sample	PCEGS[1] #	PLID[2]	Mass Quartz (g)	C yield (μg)	Diluted Mass C (μg)	AMS Split Mass C[3] (μg)	$\delta^{13}C$ (‰ VPDB[4])	$^{14}C/^{13}C$[5] (10^{-12})	$^{14}C/C_{total}$[6] (10^{-14})	^{14}C[7] (10^{5} at)	$[^{14}C]$ (10^{5} at g^{-1})
BG21-001	PCEGS-146	202101960	5.02378	5.0 ± 0.1	393.8 ± 4.8	382.3 ± 4.6	-45.9 ± 0.2	3.3992 ± 0.0745	3.4118 ± 0.0785	6.1771 ± 0.1793	1.2296 ± 0.0357
BG21-002	PCEGS-147	202101961	5.02383	7.8 ± 0.1	303.3 ± 3.7	294.4 ± 3.6	-44.8 ± 0.2	4.5548 ± 0.0964	4.6226 ± 0.1016	6.4703 ± 0.1806	1.2879 ± 0.0360
BG21-002R	PCEGS-150	202201473	5.04116	7.7 ± 0.1	305.3 ± 3.7	296.4 ± 3.6	-45.2 ± 0.2	4.5575 ± 0.1350	4.6239 ± 0.1422	6.5186 ± 0.2368	1.2931 ± 0.0470
BG21-003	PCEGS-148	202101962	5.01070	17.6 ± 0.3	303.4 ± 3.7	294.5 ± 3.6	-43.9 ± 0.2	4.6325 ± 0.1075	4.7091 ± 0.1134	6.6042 ± 0.1969	1.3180 ± 0.0393
BG21-004	PCEGS-152	202101963	5.05927	11.9 ± 0.2	305.7 ± 3.7	296.8 ± 3.6	-44.6 ± 0.2	4.6181 ± 0.0789	4.6905 ± 0.0832	6.6300 ± 0.1588	1.3105 ± 0.0314
BG21-005	PCEGS-153	202101964	5.07578	4.6 ± 0.1	304.5 ± 3.7	295.6 ± 3.6	-45.4 ± 0.2	4.5997 ± 0.1272	4.6668 ± 0.1339	6.5656 ± 0.2251	1.2935 ± 0.0444
BG21-006	PCEGS-155	202101965	5.06572	5.5 ± 0.1	306.8 ± 3.7	297.8 ± 3.6	-45.2 ± 0.2	1.2766 ± 0.0562	1.1715 ± 0.0594	1.2426 ± 0.1010	0.2453 ± 0.0199
BG21-007	PCEGS-157	202101966	5.03589	6.9 ± 0.1	309.2 ± 3.8	300.1 ± 3.7	-45.0 ± 0.2	1.6838 ± 0.0507	1.6007 ± 0.0536	1.9221 ± 0.0960	0.3817 ± 0.0191
BG21-008	PCEGS-158	202101967	5.07653	4.0 ± 0.1	308.9 ± 3.8	299.9 ± 3.6	-45.4 ± 0.2	2.3565 ± 0.0634	2.3076 ± 0.0669	3.0145 ± 0.1185	0.5938 ± 0.0234
BG21-009	PCEGS-160	202101968	5.01906	55.3 ± 0.7	305.6 ± 3.7	296.6 ± 3.6	-38.0 ± 0.2	3.3393 ± 0.0946	3.3681 ± 0.1005	4.6013 ± 0.1703	0.9168 ± 0.0339
BG21-010	PCEGS-161	202101969	4.99961	42.2 ± 0.6	306.0 ± 3.7	297.0 ± 3.6	-40.1 ± 0.2	3.3197 ± 0.0680	3.3399 ± 0.0721	4.5648 ± 0.1321	0.9130 ± 0.0264
Procedural Blanks											
PB2-03222022	PCEGS-135	202201450	--	1.4 ± 0.1	305.2 ± 3.7	296.2 ± 3.6	-40.2 ± 0.2	0.4853 ± 0.0298	0.3413 ± 0.0320	0.5222 ± 0.0493	--
PB2-04212022	PCEGS-145	202201452	--	1.8 ± 0.1	307.0 ± 3.7	298.0 ± 3.6	-46.0 ± 0.2	0.5182 ± 0.0273	0.3731 ± 0.0292	0.5742 ± 0.0455	--
PB2-05212022	PCEGS-163	202201454	--	2.3 ± 0.1	307.4 ± 3.7	298.4 ± 3.6	-46.0 ± 0.2	0.5364 ± 0.0315	0.3922 ± 0.0335	0.6045 ± 0.0521	--
PB2-06022022	PCEGS-169	202201459	--	2.3 ± 0.1	307.3 ± 3.7	298.3 ± 3.6	-40.3 ± 0.2	0.4920 ± 0.0291	0.3486 ± 0.0312	0.5371 ± 0.0486	--
									Mean ± 1σ (All blanks)	*0.5595 ± 0.0371*	
									Mean ± 1σ (145,163 only)	*0.5894 ± 0.0214*	

Notes

1 Purdue Carbon Extraction and Graphitization System.
2 Prime Lab ID.
3 Mass graphitized for AMS analysis after small aliquot (ca. 9 μg C) taken for stable C isotopic analysis offline.
4 VPDB is Vienna Peedee Belemnite.
5 Measured relative to OX-2 standard.
6 Corrected for mass-dependent graphitization blank (based on AMS Split Mass C) and stable C composition.
7 Sample values calculated using Diluted Mass C and corrected for mean procedural blank (All blanks).

335
336

Table ~~2.~~2. Apparent ~~i~~*In situ* ^{14}C ages from quartz, Dalarna-Gävleborg and Forsmark-Uppland.

Sample[1] ~~ID~~	Lat (°)	Long (°)	Elevation (m a.s.l.)	^{14}C a~~A~~ge ~~± Unc.~~[Ext.] ~~(± Unc.~~[Int.]~~)~~[2a] (ka)
BG21-001	60.47432	16.33134	236.5	10.6 ± 2.2 (± 0.6)
BG21-002	60.40615	16.22197	212.6	12.3 ± 2.9 (± 0.8)
BG21-002R	60.40615	16.22197	212.6	12.4 ± 3.0 (± 1.1)
BG21-003	60.38459	16.17649	216.3	12.9 ± 3.2 (± 0.9)
BG21-004	60.38451	16.17440	217.8	12.7 ± 3.0 (± 0.7)
BG21-005	60.36888	16.30526	248.1	11.6 ± 2.6 (± 0.9)
BG21-006	60.38490	18.22308	9.4	1.5 ± 0.2 (± 0.1)
BG21-007	60.37892	18.19129	12.2	2.6 ± 0.3 (± 0.2)
BG21-008	60.30504	18.04993	30.3	4.5 ± 0.6 (± 0.2)
BG21-009	60.22988	17.94989	56.0	8.2 ± 1.5 (± 0.5)
BG21-010	60.22431	17.95051	55.9	8.2 ± 1.4 (± 0.4)

Notes

1 All samples have a thickness of 3 cm, a density of 2.7 g cm^{-3}, and a shielding factor of 1. Zero erosion is assumed.

2 ~~a~~ ^{14}C a~~A~~ge ~~and~~ 1σ external uncertainty (1σ internal uncertainty) ~~and Unc.~~[Ext.] ~~is external uncertainty and Unc.~~[Int.] ~~is (internal uncertainty). Both are 1σ.~~

337
338
339

5. Discussion

The *in situ* ^{14}C bedrock exposure ages from the Forsmark-Uppland transect (i.e., below the highest postglacial shoreline) consistently increase with elevation and overlap the expected exposure age curve, within uncertainty (Fig. 3). ~~Because the apparent exposure ages accurately reflect the timing of landscape emergence, *in situ* ^{14}C is indicated as having high potential as a chronometer over Late Glacial-Holocene timescales in low-relief, low-elevation settings.~~ This study adds to precious few ~~demonstrations of the ability of~~ applications of cosmogenic nuclides ~~isotopes~~ to defininge postglacial landscape emergence above sea level (Briner et al., 2006; Bierman et al., 2018). Briner et al. (2006) present good (visual) congruence with a record of shoreline emergence built from radiocarbon-dated driftwood and fauna by Dyke et al. (1992) using ^{10}Be measurements on boulders in beaches derived from wave-washed till. Their study also mentions that building a relative sea level curve from pebbles, cobbles and plucked bedrock suffered from inheritance problems, an experience shared by Matmon et al. (2003) while attempting the dating of chert on beach ridges in southern Israel and heeded by Bierman et al. (2018). Bierman et al. (2018) successfully dated landscape emergence on Greenland using ^{10}Be across a range of settings, including bedrock below the highest shoreline, cobbles from beach ridges at the highest shoreline, and boulders and bedrock above the highest shoreline. They note that success hinges on the requirement of warm-based ice and deep glacial erosion in exposing bedrock devoid of an inherited cosmogenic nuclide inventory. In many regions, however, including east-central Sweden and more widely in Fennoscandia, these requirements are not met either because of cold-based conditions (Patton et al., 2016; Stroeven et al., 2016) or weakly erosive warm-based ice such as at Forsmark (Hall et al., 2019; SKB, 2020), during all or much of glacial time. Cosmogenic nuclide inheritance is therefore a part of the landscape fabric. Bierman et al. (2018) advocate the use of *in situ* ^{14}C as a methodology to circumvent inheritance problems. Our study is the first to follow-up on that suggestion, and shows, convincingly, that using *in situ* ^{14}C can extend the study of landscape rebound to regions where ice sheet erosion was insufficiently deep to allow for the application of long-lived nuclides.

Five bedrock samples from above the highest postglacial shoreline are well-clustered and the weighted mean age (and full uncertainty) of 11.9~~2~~ ± 1.5~~3~~ ka overlaps with the predicted deglaciation age of 10.8 ± 0.3 ka (Fig. 4~~a~~; Hughes et al., 2016; Stroeven et al., 2016). ~~Removing the youngest age from consideration results in more strongly clustered ages (Fig. 4b) and an older mean weighted age of 11.612.4 ± 1.31 ka, which still overlaps the predicted deglaciation age, within uncertainty. We therefore do not further discriminate between these results.~~ Because derived exposure ages overlap with the predicted deglaciation age, we further infer that the *in situ* ^{14}C samples, including those located below the highest postglacial shoreline, within uncertainty, lack significant inheritance from previous

exposure. Model scenarios of *in situ* ^{14}C concentration evolution over varying durations of MIS2 and MIS4~~3~~ ice cover ~~indicate~~are consistent with minor inheritance, even with short periods of ice coverage

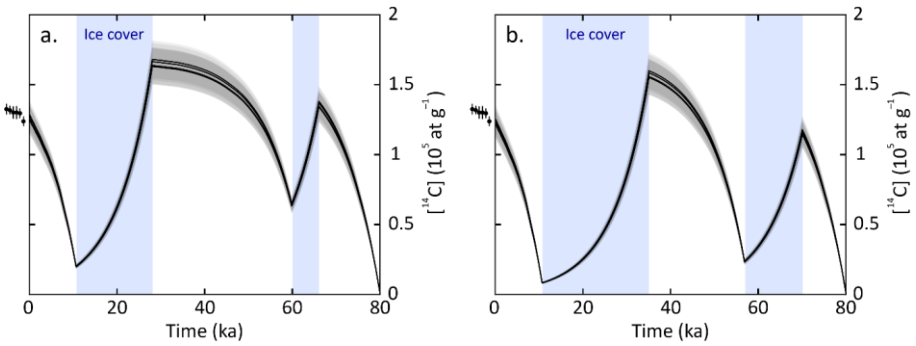

and ~~an assumption of~~ no glacial or interglacial erosion (Figure 5). ~~The apparent~~is ~~lack of inheritance in samples from above the highest shoreline implies that the last ice sheet advanced over the study area soon after 35 ka, in accordance with previous inferences for Forsmark (SKB, 2020)~~Even if the last ice sheet ~~would have~~ had advanced over the region as late as 28 ka BP, there would only be a ~~very minor~~negligible ~~amount~~inventory of inherited ^{14}C atoms produced prior to the MIS2 ice advance. ~~An alternative interpretation is that the last ice sheet advanced more recently but that glacial erosion during MIS2 was sufficiently deep to remove any nuclide inheritance.~~

Figure 5. Modelled ~~*i*~~*in situ* ^{14}C concentration evolution over the last 80 kyr ~~in bedrock surfaces through alternating periods of subaerial exposure and burial by ice sheets during MIS2 and MIS3. These histories are modelled from ^{14}C concentrations~~ in the five samples (BG21-001–BG21-005) from above the highest shoreline. ~~and assume no glacial or interglacial erosion~~ The ^{14}C development is modelled assuming no glacial or interglacial erosion, continuous exposure to cosmic rays during ice-free periods, and full shielding from cosmic rays (no ^{14}C production) during periods with ice cover. The points just left of the plots display the measured ^{14}C concentrations for the six sample measurements ~~of the samples~~ (Table 1). (a) Scenario with ~~S~~short periods of MIS4~~2~~ and MIS2~~3~~ ice cover from 66 to 60 ka BP and from 28 ka BP to ~~the time of~~ deglaciation around 10.7 ka BP. (b) Scenario with ~~L~~longer periods of MIS4~~2~~ and MIS2~~3~~ ice cover from 70 to 57 ka BP and from 35 ka BP to the deglaciation around 10.7 ka BP. Due to the rapid decay of ^{14}C (~~with a~~ half-life of 5700 ± 30 ~~5700~~ years), both scenarios yield similar ~~similar~~ end-point concentrations of ^{14}C that overlap, ~~s~~ within uncertainties, ~~with~~ the measured sample concentrations.

Our *in situ* ^{14}C data from above the highest (postglacial) shoreline demonstrate ~~good its~~their potential for ~~this nuclide to help~~ constraining the deglaciation chronology of former ice sheets. This is especially true for regions with thin ~~drift~~till drapes, abundant bedrock exposures, and sparse moraines outlining

successive retreat stages. In Fennoscandia, thin ~~drift~~ tills ~~conditions~~ occur commonly (cf. Kleman et al., 2008) and ice sheet retreat appears to have proceeded uninterrupted inside the Younger Dryas moraine belt (apart from the Central Finland Ice-Marginal Formation; e.g., Rainio et al., 1986; Stroeven et al., 2016). Whereas the post-Younger Dryas deglaciation of east-central Sweden is well constrained by clay-varve chronology below the highest postglacial shoreline (Strömberg, 1989) ~~below the highest postglacial shoreline~~, there are vast areas above the highest shoreline that remain poorly constrained by data (Stroeven et al. 2016). In addition to a lack of datable deglacial landforms, this is attributable to glacial erosion of bedrock having frequently been insufficient to remove inventories of long half-life ^{10}Be and ^{26}Al (Patton et al., 2022), thereby leaving nuclides inherited from exposure prior to the last glaciation (Heyman et al., 2011; Stroeven et al., 2016). Because of the short ^{14}C half-life and an improved sampling methodology, *in situ* ^{14}C may now be a prime candidate nuclide to be included in last deglaciation studies on glaciated cratons, such as the dating of boulders deposited along glacial flowlines; a technique practiced successfully using ^{10}Be (Margold et al., 2019; Norris et al., 2022).

6. Conclusion

Ten *in situ* ^{14}C measurements on bedrock are consistent with a RSL curve for Forsmark derived from organic radiocarbon dating of basal sediments in isolation basins and the Fennoscandian Ice Sheet deglaciation chronologies from Stroeven et al. (2016) and Hughes et al. (2016). This study introduces the use of *in situ* ^{14}C in Fennoscandian Ice Sheet paleoglaciology and outlines a promise of its use as a basis for supporting future shoreline displacement studies and for tracking the deglaciation in areas that lack datable organic material and where ^{10}Be and ^{26}Al routinely return complex exposure results.

Data availability. Data are available in Supplements 1-3. LiDAR data used in the study ~~can downloaded~~ are available from https://www.lantmateriet.se

Author contributions. BWG and APS initiated the study, with support from KH and JON, and drafted the manuscript. BWG, APS, and AL did the sampling. AL did petrological analyses of the sampled bedrock. NAL completed sample preparation for AMS and provided the results. JH carried out cosmogenic nuclide production rate and exposure age calculations. MWC oversaw the AMS. All authors revised the manuscript.

Competing interests. The contact author has declared that none of the authors has any competing interests.

Disclaimer. Publisher's note: Copernicus Publications remains neutral with regard to jurisdictional claims in published maps and institutional affiliations.

Acknowledgements. We thank Johan Liakka (SKB) for his support in completing this study and Nicolás Young and an anonymous reviewer for comments that improved this manuscript.~~-~~

Financial support. This research was supported by the Swedish Nuclear Fuel and Waste Management Company.

Review statement. This paper was edited by Pieter Vermeesch and reviewed by Nicolás Young and an anonymous reviewer.

References

Alexanderson, H., Hättestrand, M., Lindqvist, M. A., Sigfusdottir, T.: MIS 3 age of the Veiki moraine in N Sweden - Dating the landform record of an intermediate-sized ice sheet in Scandinavia, Arctic, Antarctic, and Alpine Research, 54, 239-261, 2022.

Balco, G., Stone, J. O., Lifton, N. A., Dunai, T. J.: A complete and easily accessible means of calculating surface exposure ages or erosion rates from ^{10}Be and ^{26}Al measurements, Quaternary Geochronology, 3, 174–195, 2008.

Berglund, M.: The Holocene shore displacement of Gästrikland, eastern Sweden: a contribution to the knowledge of Scandinavian glacio-isostatic uplift, Journal of Quaternary Science, 20, 519–531, 2005.

Bergström, E.: Late Holocene distribution of lake sediment and peat in NE Uppland, Sweden, SKB R-01-12, Svensk Kärnbränslehantering AB, 2001.

Bierman, P. R., Rood, D. H., Shakun, J. D., Portenga, E. W., Corbett, L. B.: Directly dating postglacial Greenlandic land-surface emergence at high resolution using in situ ^{10}Be, Quaternary Research, 90, 110-126, 2018.

Blake, Jr., W.: Holocene emergence along the Ellesmere Island coast of northernmost Baffin Bay, Norsk Geologisk Tidsskrift, 73, 147–160, 1993.

Borchers, B., Marrero, S., Balco, G., Caffee, M., Goehring, B., Lifton, N., Nishiizumi, K., Phillips, F., Schaefer, J., Stone, J.: Geological calibration of spallation production rates in the CRONUSEarth project, Quaternary Geochronology, 31, 188–198, 2016.

Bradwell, T., Fabel, D., Clark, C. D., Chiverrell, R. C., Small, D., Smedley, R. K., Saher, M. H., Moreton, S. G., Dove, D., Callard, S. L., Duller, G. A. T., Medialdea, A., Bateman, M. D., Burke, M. J., McDonald, N., Gilgannon, S., Morgan, S., Roberts, D. H., Ó Cofaigh, C.: Pattern, style and timing of British-Irish Ice Sheet advance and retreat over the last 45 000 years: evidence from NW Scotland and the adjacent continental shelf, Journal of Quaternary Science, 36, 871–933, 2021.

Briner, J. P., Gosse, J. C., Bierman, P. R.: Applications of cosmogenic nuclides to Laurentide Ice Sheet history and dynamics, Geological Society of America, Special Paper, 415, 29-41, 2006.

Briner, J. P., Lifton, N. A., Miller, G. H., Refsnider, K., Anderson, R. K., Finkel, R.: Using *in situ* cosmogenic ^{10}Be, ^{14}C, and ^{26}Al to decipher the history of polythermal ice sheets, Quaternary Geochronology, 19, 4–13, 2014.

Brunnberg, L.: Clay-varve Chronology and Deglaciation during the Younger Dryas and Preboreal in the Easternmost Part of the Middle Swedish Ice Marginal Zone, Department of Quaternary Research, Quaternaria A2, Stockholm University, Stockholm, 1-94, 1995.

Dalton, A.S., Dulfer, H.E., Margold, M., Heyman, J., Clague, J.J., Froese, D.G., Gauthier, M.S., Hughes, A.L.C., Jennings, C.E., Norris, S.L., Stoker, B.J.: Deglaciation of the north American ice sheet complex

in calendar years based on a comprehensive database of chronological data: NADI-1, Quaternary Science Reviews, 321, 108345, 2023.

Dalton, A. S., Margold, M., Stokes, C. R., Tarasov, L., Dyke, A. S., Adams, R. S., Allard, S., Arends, H. E., Atkinson, N., Attig, J. W., Barnett, P. J., Barnett, R. L., Batterson, M., Bernatchez, P., Borns Jr., H. W., Breckenridge, A., Briner, J. P., Brouard, E., Campbell, J. E., Carlson, A. E., Clague, J. J., Curry, B. B., Daigneault, R. A., Dubé-Loubert, H., Easterbrook, D. J., Franzi, D. A., Friedrich, H. G., Funder, S., Gauthier, M. S., Gowan, A. S., Harris, K. L., Hétu, B., Hooyer, T. S., Jennings, C. E., Johnson, M. D., Kehew, A. E., Kelley, S. E., Kerr, D., King, E. L., Kjeldsen, K. K., Knaeble, A. R., Lajeunesse, P., Lakeman, T. R., Lamothe, M., Larson, P., Lavoie, M., Loope, H. M., Lowell, T. V., Lusardi, B. A., Manz, L., McMartin, I., Nixon, F. C., Occhietti, S., Parkhill, M. A., Piper, D. J. W., Pronk, A. G., Richard, P. J. H., Ridge, J. C., Ross, M., Roy, M., Seaman, A., Shaw, J., Stea, R. R., Teller, J. T., Thompson, W. B., Thorleifson, L. H., Utting, D. J., Veillette, J. J., Ward, B. C., Weddle, T. K., Wright, H. E.: An updated radiocarbon-based ice margin chronology for the last deglaciation of the North American Ice Sheet Complex, Quaternary Science Reviews, 234, 106223, 2020.

De Geer, G.: The transbaltic extension of the Swedish Time Scale, Geografiska Annaler, 17, 533-549, 1935.

De Geer, G.: Geochronologia Suecica principles, Kungliga svenska vetenskapsakademien Handlingar, III, Bd 18, 6, 1–367, 1940.

Dyke, A. S., Morris, T. F., Green, D. E. C., England, J.: Quaternary geology of Prince of Wales Island, Arctic Canada, Geological Survey of Canada, Memoir, 433, 1–142, 1992.

Dyke, A. S., Andrews, J. T., Clark, P. U., England, J. H., Miller, G. H., Shaw, J., Veillette, J. J.: The Laurentide and Innuitian ice sheets during the Last Glacial Maximum, Quaternary Science Reviews, 21, 9–31, 2002.

Fogwill, C., Turney, C., Golledge, N., Rood, D., Hippe, K., Wacker, L., Jones, R.: Drivers of abrupt Holocene shifts in West Antarctic ice stream direction determined from combined ice sheet modelling and geologic signatures. Antarctic Science, 26, 674–686, 2014.

Goehring, B. M., Schaefer, J. M., Schluechter, C., Lifton, N. A., Finkel, R. C., Jull, A. J. T., Akçar, N., Alley, R. B.: The Rhone Glacier was smaller than today for most of the Holocene, Geology, 39, 679–682, 2011.

Gosse, J. C., Phillips, F. M.: Terrestrial *in situ* cosmogenic nuclides: theory and application, Quaternary Science Reviews, 20, 1475–1560, 2001.

Greenwood, S. L., Simkins, L. M., Winsborrow, M. C. M., Bjarnadottir, L. R.: Exceptions to bed-controlled ice sheet flow and retreat from glaciated continental margins worldwide, Science Advances, 7, eabb6291, 2021.

Greenwood, S. L., Clason, C. C., Nyberg, J., Jakobsson, M., Holmlund, P.: The Bothnian Sea ice stream: early Holocene retreat dynamics of the south-central Fennoscandian Ice Sheet, Boreas, 46, 346-362, 2017.

Hall A. M., Ebert K., Goodfellow B. W., Hättestrand C., Heyman J., Krabbendam M., Moon S., Stroeven A. P.: Past and future impact of glacial erosion in Forsmark and Uppland. TR-19-07 Svensk Kärnbränslehantering AB, 2019.

514 Hall, A. M., Krabbendam, M., van Boeckel, M., Goodfellow, B. W., Hättestrand, C., Heyman, J.,
515 Palamakumbura, R. N., Stroeven A. P., Näslund, J.-O.: Glacial ripping: geomorphological evidence
516 from Sweden for a new process of glacial erosion, Geografiska Annaler, 102, 333-353, 2020.

517 Hedenström, A., Risberg, J.: Shore displacement in northern Uppland during the last 6500 calender
518 years, TR-03-17 Svensk Kärnbränslehantering AB, 2003.

519 Heyman, J., Stroeven, A. P., Harbor, J. M., Caffee, M. W.: Too young or too old: Evaluating
520 cosmogenic exposure dating based on an analysis of compiled boulder exposure ages, Earth and
521 Planetary Science Letters, 302, 71–80, 2011.

522 Hippe, K., Lifton, N. A.: Calculating isotope ratios and nuclide concentrations for *in situ* cosmogenic
523 ^{14}C Analyses, Radiocarbon, 56, 1167–1174, 2014.

524 Hippe, K., Ivy-Ochs, S., Kober, F., Zasadni, J., Wieler, R., Wacker, L., Kubik, P.W., Schlüchter, C.:
525 Chronology of Lateglacial ice flow reorganization and deglaciation in the Gotthard Pass area, Central
526 Swiss Alps, based on cosmogenic ^{10}Be and *in situ* ^{14}C, Quaternary Geochronology, 19, 14–26, 2014.

527 Hughes, A. L. C., Gyllencreutz, R., Lohne, Ø. S., Mangerud, J., Svendsen, J. I.: The last Eurasian ice
528 sheets – a chronological database and time-slice reconstruction, DATED-1, Boreas, 45, 1–45, 2016.

529 Ivy-Ochs, S., Kober, F.: Surface exposure dating with cosmogenic nuclides, Quaternary Science
530 Journal, 57, 157–189, 2008.

531 Kleman, J., Hättestrand, M., Borgström, I., Preusser, F., Fabel, D.: The Idre marginal moraine–an
532 anchorpoint for Middle and Late Weichselian ice sheet chronology, Quaternary Science Advances, 2,
533 100010, 2020.

534 Kleman, J., Stroeven, A. P., Lundqvist, J.: Patterns of Quaternary ice sheet erosion and deposition in
535 Fennoscandia and a theoretical framework for explanation, Geomorphology, 97, 73–90, 2008.

536 Koester, A., Lifton, N. A.: Technical note: A software framework for calculating compositionally
537 dependent *in situ* ^{14}C production rates, Geochronology, 5, 21–33, 2023.

538 Lal, D.: Cosmic ray labeling of erosion surfaces: *in situ* nuclide production rates and erosion rates,
539 Earth and Planetary Science Letters, 104, 424–439, 1991.

540 Lambeck, K., Purcell, A., Zhao, J., Svensson, N.-O.: The Scandinavian Ice Sheet: from MIS 4 to the end
541 of the Last Glacial Maximum, Boreas, 39, 410-435, 2010.

542 Lambeck, K., Smither, C., Johnston, P.: Sea-level change, glacial rebound and mantle viscosity for
543 northern Europe, Geophysical Journal International, 134, 102-134, 1998.

544 Lidberg, M., Johansson, J. M., Scherneck, H.-G., Milne, G. A.: Recent results based on continuous GPS
545 observations of the GIA process in Fennoscandia from BIFROST, Journal of Geodynamics, 50, 8–18,
546 2010.

547 Lifton, N.: Implications of two Holocene time-dependent geomagnetic models for cosmogenic nuclide
548 production rate scaling, Earth and Planetary Science Letters, 433, 257–268, 2016.

549 Lifton, N., Caffee, M., Finkel, R., Marrero, S., Nishiizumi, K., Phillips, F. M., Goehring, B., Gosse, J.,
550 Stone, J., Schaefer, J., Theriault, B.: *In situ* cosmogenic nuclide production rate calibration for the
551 CRONUS-Earth project from Lake Bonneville, Utah, shoreline features, Quaternary Geochronology,
552 26, 56–69, 2015.

Lifton, N., Sato, T., and Dunai, T. J.: Scaling *in situ* cosmogenic nuclide production rates using analytical approximations to atmospheric cosmic-ray fluxes, Earth and Planetary Science Letters, 386, 149–160, 2014.

Lifton, N., Wilson, J., Koester. A.: Technical note: Studying Li-metaborate fluxes and extraction protocols with a new, fully automated *in situ* cosmogenic ^{14}C processing system at PRIME Lab, Geochronology, 5, 361–375, 2023.

Long, A. J., Woodroffe, S. A., Roberts, D. H., Dawson, S.: Isolation basins, sea-level changes and the Holocene history of the Greenland Ice Sheet, Quaternary Science Reviews, 30, 3748–3768, 2011.

Lönnqvist, M., Hökmark, H.: Approach to estimating the maximum depth for glacially induced hydraulic jacking in fractured crystalline rock at Forsmark, Sweden, Journal of Geophysical Research: Earth Surface, 118, 1777–1791, 2013.

Lupker, M., Hippe, K., Wacker, L., Kober, F., Maden, C., Braucher, R., Bourlès, D., Romani, J. R. V., Wieler, R.: Depth-dependence of the production rate of *in situ* ^{14}C in quartz from the Leymon High core, Spain, Quaternary Geochronology, 28, 80–87, 2015.

Margold, M., Gosse, J. C., Hidy, A. J., Woywitka, R. J., Young, J. M., Froese, D.: Beryllium-10 dating of the Foothills Erratics Train in Alberta, Canada, indicates detachment of the Laurentide Ice Sheet from the Rocky Mountains at ~15 ka, Quaternary Research, 92, 469–482, 2019.

Marrero, S. M., Phillips, F. M., Caffee, M. W., Gosse, J. C.: CRONUS-Earth cosmogenic ^{36}Cl calibration, Quaternary Geochronology, 31, 199–219, 2016.

Matmon, A., Crouvi, O., Enzel, Y., Bierman, P., Larsen, J., Porat, N., Amit, R., Caffee, M.: Complex exposure histories of chert clasts in the late Pleistocene shorelines of Lake Lisan, southern Israel. Earth Surface Processes and Landforms 28, 493–506, 2003.

Miller, G. H., Briner, J. P., Lifton, N. A., Finkel, R. C.: Limited ice-sheet erosion and complex exposure histories derived from *in situ* cosmogenic ^{10}Be, ^{26}Al, ^{14}C on Baffin Island, Arctic Canada, Quaternary Geochronology, 1, 74–85, 2006.

Moon, S., Perron, J. T., Martel, S.J., Goodfellow, B.W., Mas Ivars, D., Hall, A., Heyman, J., Munier, R., Näslund, J.-O., Simeonov, A., Stroeven, A.P.: Present-day stress field influences bedrock fracture openness deep into the subsurface. *Geophysical Research Letters* 47, e2020GL090581, 2020.

Norris, S. L., Tarasov, L., Monteath, A. J., Gosse, J. C., Hidy, A. J., Margold, M., Froese, D. G.: Rapid retreat of the southwestern Laurentide Ice Sheet during the Bølling-Allerød interval, Geology, 50, 417–421, 2022.

Påsse, T., Andersson, L: Shore-level displacement in Fennoscandia calculated from empirical data, GFF, 127, 253–268, 2005.

Patton, H., Hubbard, A., Andreassen, K., Auriac, A., Whitehouse, P. L., Stroeven, A. P., Shackleton, C., Winsborrow, M., Heyman, J., Hall, A. M.: Deglaciation of the Eurasian ice sheet complex, Quaternary Science Reviews, 169, 148–172, 2017.

Patton, H., Hubbard, A., Andreassen, K., Winsborrow, M., Stroeven, A.P.: The build-up, configuration, and dynamical sensitivity of the Eurasian ice-sheet complex to Late Weichselian climatic and oceanic forcing, Quaternary Science Reviews, 153, 97–121, 2016.

592 Patton, H., Hubbard, A., Heyman, J., Alexandropoulou, N., Lasabuda, A. P. E., Stroeven, A.P., Hall,
593 A.M., Winsborrow, M., Sugden, D.E., Kleman, J., Andreassen, K.: The extreme yet transient nature of
594 glacial erosion, Nature Communications 13, 7377, 2022.

595 Pendleton, S., Miller, G., Lifton, N., Young, N.: Cryosphere response resolves conflicting evidence for
596 the timing of peak Holocene warmth on Baffin Island, Arctic Canada, Quaternary Science
597 Reviews, 216, 107–115, 2019.

598 Phillips, F. M., Argento, D. C., Balco, G., Caffee, M. W., Clem, J., Dunai, T. J., Finkel, R., Goehring, B.,
599 Gosse, J. C., Hudson, A. M., Jull, A. J. T., Kelly, M. A., Kurz, M., Lal, D., Lifton, N., Marrero, S. M.,
600 Nishiizumi, K., Reedy, R. C., Schaefer, J., Stone, J. O. H., Swanson, T., Zreda, M. G.: The CRONUS-Earth
601 Project: A synthesis, Quaternary Geochronology, 31, 119–154, 2016.

602 Rainio, H., Kejonen, A., Kielosto, S., Lahermo, P.: Avancerade inlandsisen på nytt också till
603 Mellanfinska randformationen? Geologi, 38, 95–109, 1986.

604 Regnéll, C., Becher, G. P., Öhrling, C., Greenwood, S. L., Gyllencreutz, R., Blomdin, R., Brendryen, J.,
605 Goodfellow, B. W., Mikko, H., Ransed, G., Smith, C.: Ice-dammed lakes and deglaciation history of the
606 Scandinavian Ice Sheet in central Jämtland, Sweden, Quaternary Science Reviews, 314, 108219, 2023.

607 Risberg, J.: Strandförskjutningen i nordvästra Uppland under subboreal tid. In Segerberg, A. Bälinge
608 mossar: kustbor i Uppland under yngre stenålder, PhD Thesis. Uppsala University, Appendix 4. (in
609 Swedish), 1999.

610 Robertsson, A.-M., Persson, C.: Biostratigraphical studies of three mires in northern Uppland,
611 Sweden, Sveriges geologiska undersökning, (Serie C 821.), 1989.

612 Romundset, A., Bondevik, S., Bennike, O.: Postglacial uplift and relative sea level changes in
613 Finnmark, northern Norway, Quaternary Science Reviews, 30, 2398–2421, 2011.

614 Schildgen, T. F., Phillips, W. M., Purves, R. S.: Simulation of snow shielding corrections for cosmogenic
615 nuclide surface exposure studies, Geomorphology, 64, 67–85, 2005.

616 Schimmelpfennig, I., Schaefer, J. M., Goehring, B. M., Lifton, N., Putnam, A. E., Barrell, D. J.:
617 Calibration of the *in situ* cosmogenic ^{14}C production rate in New Zealand's Southern Alps, Journal of
618 Quaternary Science, 27, 671–674, 2012.

619 Schimmelpfennig, I., Schaefer, J. M., Lamp, J., Godard, V., Schwartz, R., Bard, E., Tuna, T., Akçar, N.,
620 Schlüchter, C., Zimmerman, S., and ASTER Team: Glacier response to Holocene warmth inferred from
621 *in situ* ^{10}Be and ^{14}C bedrock analyses in Steingletscher's forefield (central Swiss Alps), Climate of the
622 Past, 18, 23–44, 2022.

623 Schweinsberg, A. D., Briner, J. P., Miller, G. H., Lifton, N. A., Bennike, O., & Graham, B. L.: Holocene
624 mountain glacier history in the Sukkertoppen Iskappe area, southwest Greenland, Quaternary
625 Science Reviews, 197, 142–161, 2018.

626 SGU: Högsta Kustlinjen (in Swedish) https://resource.sgu.se/dokument/produkter/hogsta-kustlinjen-
627 beskrivning (Geological Survey of Sweden), 2015.

628 Simkins, L. M., Simms, A. R., DeWitt, R.: Relative sea-level history of Marguerite Bay, Antarctic
629 Peninsula derived from optically stimulated luminescence-dated beach cobbles, Quaternary Science
630 Reviews, 77, 141–155, 2013.

SKB: Post-closure safety for the final repository for spent nuclear fuel at Forsmark – Climate and climate-related issues, PSAR version, TR-20-12, Svensk Kärnbränslehantering AB, 2020.

SKB: Post-closure safety for the final repository for spent nuclear fuel at Forsmark – Main report, PSAR version. SKB TR-21-01, Svensk Kärnbränslehantering AB, 2022.

Steffen, H., Wu, P.: Glacial isostatic adjustment in Fennoscandia - A review of data and modeling, Journal of Geodynamics, 52, 169–204, 2011.

Steinemann, O., Ivy-Ochs, S., Hippe, K., Christl, M., Haghipour, N., and Synal, H. A.: Glacial erosion by the Trift glacier (Switzerland): Deciphering the development of riegels, rock basins and gorges, Geomorphology, 375, 107533, 2021.

Stephens, M. B., Jansson, N. F.: Chapter 6, Paleoproterozoic (1.9–1.8 Ga) syn-orogenic magmatism, sedimentation and mineralization in the Bergslagen lithotectonic unit, Svecokarelian orogen. In M B Stephens & J Bergman Weihed (eds.): Sweden: Lithotectonic Framework, Tectonic Evolution and Mineral Resources, Geological Society of London Memoirs, 50, 105–206, 2020.

Stroeven, A. P., Hättestrand, C., Kleman, J., Heyman, J., Fabel, D., Fredin, O., Goodfellow, B. W., Harbor, J. M., Jansen, J. D., Olsen, L., Caffee, M. W., Fink, D., Lundqvist, J., Rosqvist, G. C., Strömberg, B., Jansson, K. N.: Deglaciation of Fennoscandia, Quaternary Science Reviews, 147, 91–12, 2016.

Stroeven, A.P., Heyman, J., Fabel, D., Björck, S., Caffee, M.W., Fredin, O., Harbor, J.M.: A new Scandinavian reference ^{10}Be production rate, Quaternary Geochronology, 29, 104–115, 2015.

Strömberg, B.: Late Weichselian deglaciation and clay varve chronology in east-central Sweden, Sveriges geologiska undersökning (Ser. Ca 73), 1989.

Strömberg, B.: Younger Dryas deglaciation at Mt. Billingen, and clay varve dating of the Younger Dryas/Preboreal transition, Boreas, 23, 177-193, 1994.

Wohlfarth, B., Björck, S., Possnert, G.: The Swedish Time Scale: a potential calibration tool for the radiocarbon time scale during the late Weichselian, Radiocarbon, 37, 347-359, 1995.

Young, N. E., Lesnek, A. J., Cuzzone, J. K., Briner, J. P., Badgeley, J. A., Balter-Kennedy, A., Graham, B. L., Cluett, A., Lamp, J. L., Schwartz, R., Tuna, T., Bard, E., Caffee, M. W., Zimmerman, S. R. H., Schaefer, J. M.: *In situ* cosmogenic ^{10}Be–^{14}C–^{26}Al measurements from recently deglaciated bedrock as a new tool to decipher changes in Greenland Ice Sheet size, Climate of the Past, 17, 419–450, 2021.

Young, N. E., Schaefer, J. M., Goehring, B., Lifton, N., Schimmelpfennig, I., Briner, J. P.: West Greenland and global *in situ* ^{14}C production-rate calibrations, Journal of Quaternary Science, 29, 401–406, 2014.